Tellus (1984), *36B*, 303–316

A study of the errors due to temporal sampling of the earth's radiation budget

By CHRISTOPHER F. ENGLAND and GARRY E. HUNT *Centre for Remote Sensing* and *Atmospheric Physics Group, Imperial College, London SW7 2AZ, England*

(Manuscript received September 27, 1983; in final form May 8, 1984)

ABSTRACT

We present results of an investigation into the errors induced in estimates of the daily mean infrared and visible fluxes due to the effects of temporal sampling over a range of spatial scales. For polar orbiting satellites, the errors are a direct consequence of the fixed local time sampling from the sun-synchronous orbit, and the poor sampling of cloud variability. Geostationary satellites, whilst providing good temporal sampling, produce vast amounts of data leading to constraints on the data handling facilities. Sampling of this geostationary data provides a means of overcoming this problem, but leads to errors similar to those experienced with polar orbiter data. In this paper, we present results of studies of the errors due to sampling at fixed intervals in universal time and those due to sampling at fixed local times, appropriate to both types of satellite system, for a wide range of surfaces and latitudes. These errors were calculated by comparing results from an hourly METEOSAT dataset with suitably sampled subsets, for April 25th, 1978.

The results show a strong latitudinal variation of error, associated with differing circulation regimes, together with a strong dependence on the local time of sampling, minimum errors occurring when sampling at 0900 and 2100 LT. Errors are most significant for the visible region of the spectrum, and are primarily due to variations in cloud cover.

1. Introduction

Accurate measurements of the Earth's radiation budget extending over a period of years, and ultimately decades, are required to monitor the variation in the driving mechanism of the weather systems, which may then relate to changes in the general circulation. Observations of radiation budget parameters have been made for nearly two decades, from a variety of spacecraft platforms (for example, Vonder Haar and Suomi, 1971; Gruber and Winston, 1978; Raschke et al., 1973; Stephens et al., 1981). All such observations have been made with sun-synchronous, polar orbiting spacecraft, which sample each location at a fixed local, and thereby introduce an aliasing error into the derived physical parameters. Attempts by Stephens et al. (1981) to investigate inter-annual variations of the Earth's radiation budget from measurements made from sensors mounted on several successive spacecraft are faced with the differing equator crossing times of each spacecraft. Only one long-term dataset, comprising 8 years of Nimbus 6 & 7 observations exists with a single equator crossing line, and even with this dataset, the magnitude of the sampling error is unknown. As a consequence, it is not yet possible to investigate the possible variations in the existing radiation budget climatologies, since no attempts have been made to assess the sources and magnitudes of errors introduced by the limitations in temporal and spatial sampling introduced by measurements from a single space platform.

In this paper, we have investigated the errors induced in estimations of the daily mean infrared and visible fluxes due to the effects of temporal sampling over a range of spatial scales. These errors may be caused by four different processes: changes in cloudiness, variations in atmospheric composition and temperature structure due to

advective and convective processes, diurnal temperature variations, particularly over the land, and changes in the atmospheric optical depth and surface albedo with solar zenith angle. For polar orbiting satellites, these errors are a direct consequence of the 12-hourly sampling by a single satellite in sun-synchronous polar orbit. Geostationary satellites have a high temporal sampling of the atmosphere, and in the case of METEOSAT observations every 30 min. This provides a further difficulty with the large amount of data that are produced daily, which for METEOSAT amounts to 1800 Mbytes/day. While the geostationary observations do provide improved sampling of the diurnal variations of atmospheric properties, the huge amount of data they produce places enormous constraints on the processing requirements of the data analysis facility, which may be reduced by sampling the data. As a consequence, we used radiation budget estimates from METEOSAT data to assess the overall accuracy of polar orbiter measurements, to determine the optimum satellite equator crossing times, and to assess the overall requirements for the data processing of geostationary observations to achieve specified accuracies.

The effect of such sampling has been discussed briefly by Saunders et al. (1983) in an intercomparison of retrievals from three satellite systems. However, the values presented are appropriate for a small number of very localised regions and are not statistically significant. Other studies have concentrated on the atmospheric variability (e.g. Saunders and Hunt, 1983; Minnis and Harrison, 1983), generally for relatively small regions, from which estimates of these effects on satellite measurement accuracy may be derived. However, at present no overall assessment of these errors has been made. The study discussed in this paper, although based upon the data for a single (typical) day, derives a significant measure of these errors, through the large spatial coverage. Radiation budget and climatic anomalies, which would perturb the results for smaller areas, are generally caused by small deviations in the tracks of travelling systems, with a greater degree of uniformity on the larger scales. Similarly, the zonal nature of the atmospheric flow indicates that considering mean zonal errors is in many ways equivalent to studying smaller areas over longer time scales, increasing the generality of the results.

Both aspects of temporal sampling are investigated using hourly measurements from METEOSAT 1. The effects of sampling at fixed intervals in universal time and the errors due to sampling at fixed local time with 12-hourly separation, that is the errors involved in using polar orbiter data, and the variation of these sampling errors with spatial extent are discussed. In both cases, the accuracy of inferred daily means is discussed in terms of the underlying surface and as a function of latitude.

2. Data

METEOSAT 1-hourly imaging data (simultaneous 11 micron infrared and visible images has been used to derive radiation budget parameters (albedo, outgoing infrared irradiance and cloud amount) on a 1 × 1 degree latitude/longitude grid. The procedure used to derive the irradiances is described in Saunders et al. (1983), using new bi-directional reflectance coefficients derived from the Numbus-7 ERB (Taylor and Stowe, 1983) to allow for the anisotropic reflectance of natural surfaces. The surface type discrimination has been improved through the incorporation of a thresholding scheme to differentiate between land and sea in coastal regions. This discrimination is necessary for the calibration of the visible images, as the satellite sensor has a triangular spectral response making the calibration a function of the surface colour.

The derived parameters were produced for an area of 120 × 120 degrees square, which is essentially the whole earth disk as seen from METEOSAT, for all of the available hourly slots on April 25, 1978. Missing slots were linearly interpolated in infrared flux density and albedo to generate a complete 24 hour dataset for subsequent resampling.

3. Methodology

3.1. *Universal time sampling: derivation of daily mean irradiances and sampling errors*

Daily mean flux densities for the visible and infrared were generated from the hourly dataset for sampling periods of 1, 2, 3, 4 5 and 6 h (including all local times within the field of view of the satellite). The sampled data were spatially averaged

to areas of 1 × 1, 2 × 2, 3 × 3, 4 × 4 and 5 × 5 degree latitude/longitude. The methodology for the sampling is discussed below.

For the derivation of mean infrared irradiances, the instantaneous irradiances were sampled directly in universal time, and the arithmetic mean of the appropriate samples was computed. The daily mean infrared irradiance, $\bar{F}_{IR}$ is therefore defined as;

$$\bar{F}_{IR} = \frac{1}{n} \sum_{i=i}^{n} F_{IR}(t_i), \tag{1}$$

where n is the number of samples per day, $F_{IR}(t_i)$ is the instantaneous flux at time t_i, with t incrementing in steps of $24/n$. The mean visible irradiance was calculated by similarly sampling the albedo and linearly interpolating this value to 15 min centres, before integrating with the calculated, instantaneous available solar irradiance. The use of the albedo, rather than a direct averaging of the measured irradiances, was necessitated by the poor sampling of the rapidly changing solar zenith angle. At periods near dawn/dusk an error will arise in the calculation due to the lack of an albedo measurement at the previous/following time step, when the satellite was sampling within the nighttime region. There are four ways in which this might be overcome, namely by:

(a) inferring the dawn/dusk albedo from climatology, with the aid of the measured infrared irradiances to determine cloud amount;

(b) extrapolating the earliest/latest measurements of albedo backwards/forwards in time to derive the dawn/dusk value;

(c) assuming that the albedo is constant from dawn/dusk to the first/final sampled measurement of the day and;

(d) by employing a climatological albedo relevant to the time, season and location.

The use of any of these techniques, however, produces errors which are dependent on the algorithm, which will vary as a function of location, and the derived error will then not be solely a function of the sampling interval, as desired. To overcome this problem of algorithm dependent error, the dawn/dusk albedo was taken to be the satellite measured value closest to the relevant time. The effect of this on the computed errors will be negligible for short period sampling, as the overall contribution of one measurement to the daily mean is small, and the available solar irradiance is low over the period in which the derived values will influence the mean. For longer time periods the effect of this simplification will be to reduce the derived error slightly although considerations of the available solar irradiance indicate that this effect will still be low (especially as the results are appropriate to all local times).

The daily mean absorbed visible irradiance $\bar{F}_{VIS}$ may thus be defined as

$$\bar{F}_{VIS} = \tfrac{1}{96} \sum_{i=i}^{96} (i - a(t_i))\, S(t_i), \tag{2}$$

where $a(t_i)$ is the interpolated albedo at time t_i subject to the consideration given above, $S(t_i)$ is the calculated instantaneous available solar irradiance.

Using these methods, the fluxes were derived for the sampling intervals discussed above, on a 1 × 1 degree latitude/longitude grid. The data were then averaged down to the required spatial scales, and binned into 10° latitude swaths. The sampling error was derived as the root mean square deviation between the hourly sampled data and the longer period sampling, on the same spatial grid within the appropriate latitude band.

3.2. *Local time sampling; derivation of daily mean flux densities*

The daily mean irradiances were obtained in a manner similar to those for the universal time sampling, except now the data were sampled in local time. The derivation of visible irradiance values differed in the albedo calculation, as the procedure used previously for the dawn/dusk region would produce unacceptable deviations from a real sampling case. In this instance, the first/last 'measured' value was assumed to be equal to that at dawn/dusk. That is, the albedo was assumed constant between dawn/dusk and the first/last 'measured' value. In many cases, this means that only a single albedo was derived for 12-hourly sampling. This is the only appropriate method for use with data sampled at 12-hourly centres, as the uncertainty of albedo estimation based on the methods described above would create major errors, given the timespan over which it must be applied. The definitions given in sub section 3.1 for universal time sampling still apply, however, with local time replacing universal time and albedos

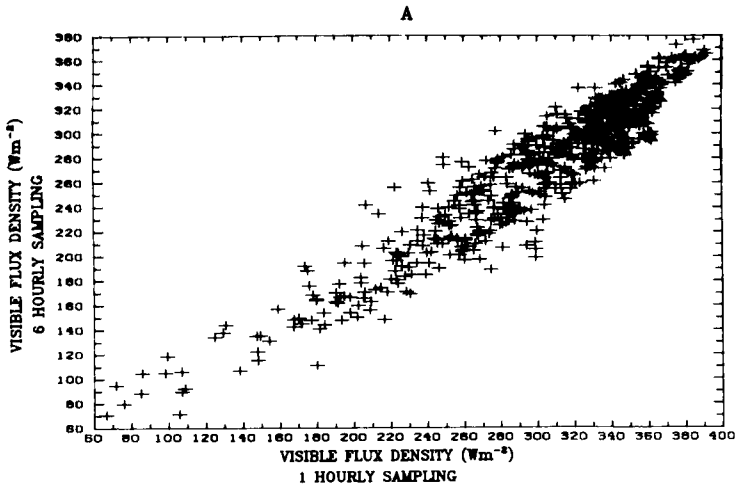
A
VISIBLE FLUX DENSITY (Wm⁻²)
6 HOURLY SAMPLING
VISIBLE FLUX DENSITY (Wm⁻²)
1 HOURLY SAMPLING

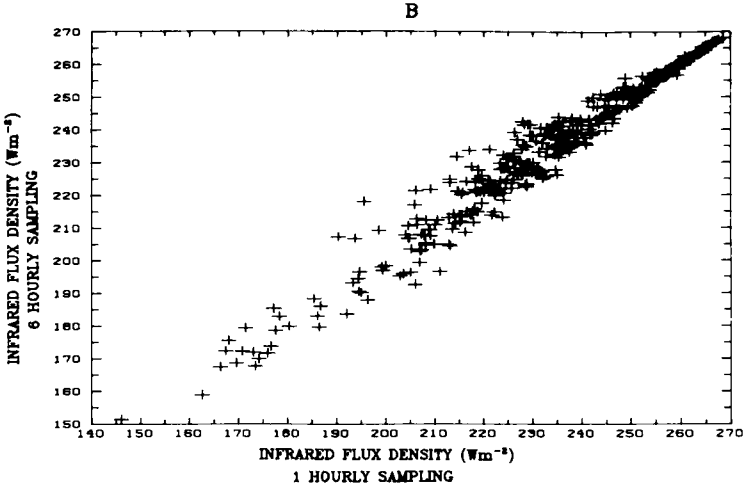
B
INFRARED FLUX DENSITY (Wm⁻²)
6 HOURLY SAMPLING
INFRARED FLUX DENSITY (Wm⁻²)
1 HOURLY SAMPLING

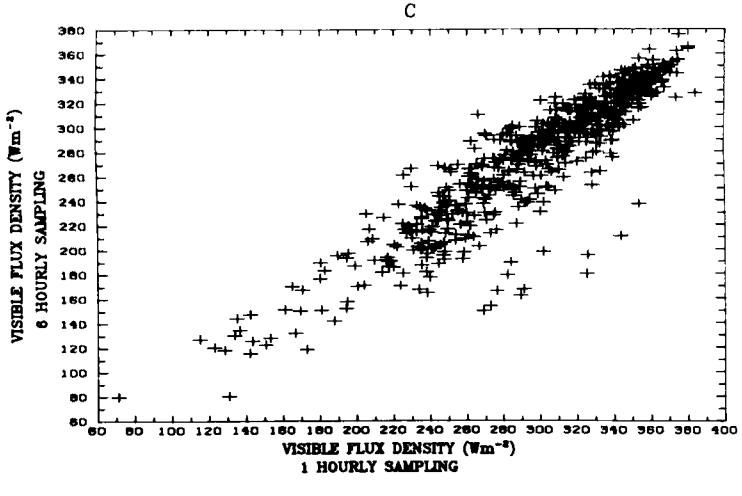
C
VISIBLE FLUX DENSITY (Wm⁻²)
6 HOURLY SAMPLING
VISIBLE FLUX DENSITY (Wm⁻²)
1 HOURLY SAMPLING

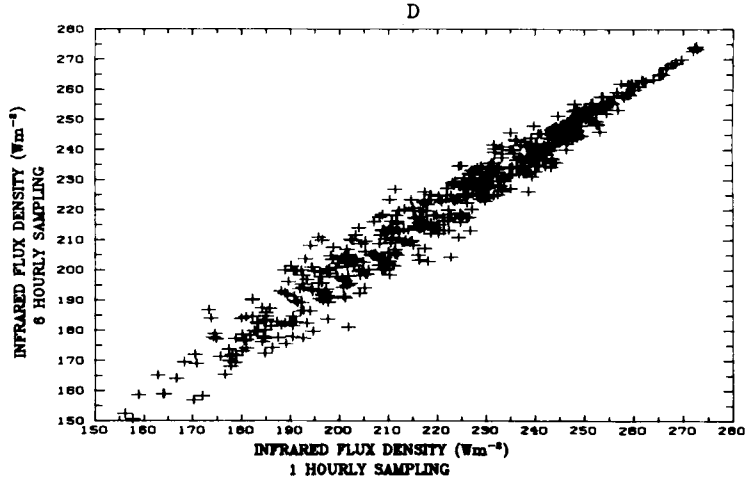
D
INFRARED FLUX DENSITY (Wm⁻²)
6 HOURLY SAMPLING
INFRARED FLUX DENSITY (Wm⁻²)
1 HOURLY SAMPLING

derived as by the method previously described. The local time, LT, is now defined as;

$$LT = UT + \text{longitude}/15$$

with

UT = Greenwich Mean Time

longitude being measured in degrees (east positive).

The sampling was performed at intervals of 12 h, and 6 h, simulating the behaviour of both a single polar orbiter and a pair of such satellites 90° out of phase. Sampling was performed on 1-hourly centres, with a spread of +/− half an hour in local time. The data do not, therefore, mimic exactly the polar orbiter sampling, since these satellites complete an orbit in approximately 100 min, with a sampling range of half this value. However, an individual pixel is sampled at the same rate (once every 12 h from a single satellite) as the sampling performed here, and thus the sampling error will be the same for a true polar orbiting satellite as that simulated here. The reduced range for the simulation was chosen as this region, for a real satellite system, encompasses the area of high spatial resolution for polar orbiting systems and hence better radiation parameter retrieval.

4. Results

4.1. *Universal time sampling*

Figs. 1a–d show the scatter produced by 6-hourly sampling, for 1 × 1 degree areas at 5*N*, for both frequency ranges over the land and sea. The data suggest strongly that a major source of the error is due to cloud variability, as the greatest deviations occur in the centre of the graph with the visible deviation much greater than the infrared. The narrowness of the scatter at 250–270 W m^{-2} in Fig. 1b may be explained if the regions of highest radiance are assumed to be due to cloud free areas, whilst the lowest radiances correspond to those that are completely cloud filled. Variability is to be expected for the central region of the graph (1930–230 W m^{-2}), where the data-points correspond to regions of either partial or variable cloudiness, which is as observed. The large difference in error between infrared and visible irradiance is difficult to explain in terms of atmospheric optical depth variation, as in this instance the two would be expected to show similar variance. Moreover, the greater variation of visible measurements over the land surfaces indicates that diurnal heating of the surface is not providing a major contribution to the sampling error. This effect is just what would be expected if cloud is the major influence, however, since the albedo may change by greater than 50% for a change from clear to cloudy conditions, with a corresponding large difference in visible irradiance. The infrared will not show a significant change, however, particularly if the cloud is low, as the temperature of the radiating surface will show little change, at most a few degrees. Furthermore, the outgoing irradiance varies approximately with temperature in the 11 micron window, where the greatest effect will occur and from which the total outgoing irradiance was inferred.

Figs. 2a, b show the variation of error in the infrared and visible irradiances as a function of latitude, for 5 × 5 degree square areas at 6-hourly sampling. The errors for the infrared flux show only slight variation with latitude, having a typical value of 3 W m^{-2}, and a range of 1.5 W m^{-2} over the ocean. Errors for the visible irradiance are higher (typically 25 W m^{-2}), with a similar range (15 W m^{-2}) over land and ocean. These show a much larger latitudinal variation than the errors in the infrared. In both cases this seems to be readily explainable in terms of meteorological phenomena. High errors in the region of the mid-latitude westerlies due to travelling depressions, with a decrease equatorwards as the weather systems become more stable with a sudden increase in error/variability in the strongly convective region of the ITCZ. The visible flux shows a decrease towards high latitudes, particularly in the southern hemisphere where this is believed to be due to the reduced insolation, but also in the north where the increased daylength gives better sampling.

Figs. 3a, b show the variation of error with increasing sampling interval for a 5 × 5 degree

Fig. 1. Comparison of radiation budget parameters sampled at 6-hourly intervals with those obtained by sampling at 1-hourly intervals for 1 degree square regions about 5° N latitude (a) Visible flux density over the ocean, (b) Infrared flux density over the ocean, (c) Visible flux density over the land, (d) Infrared flux density over the land.

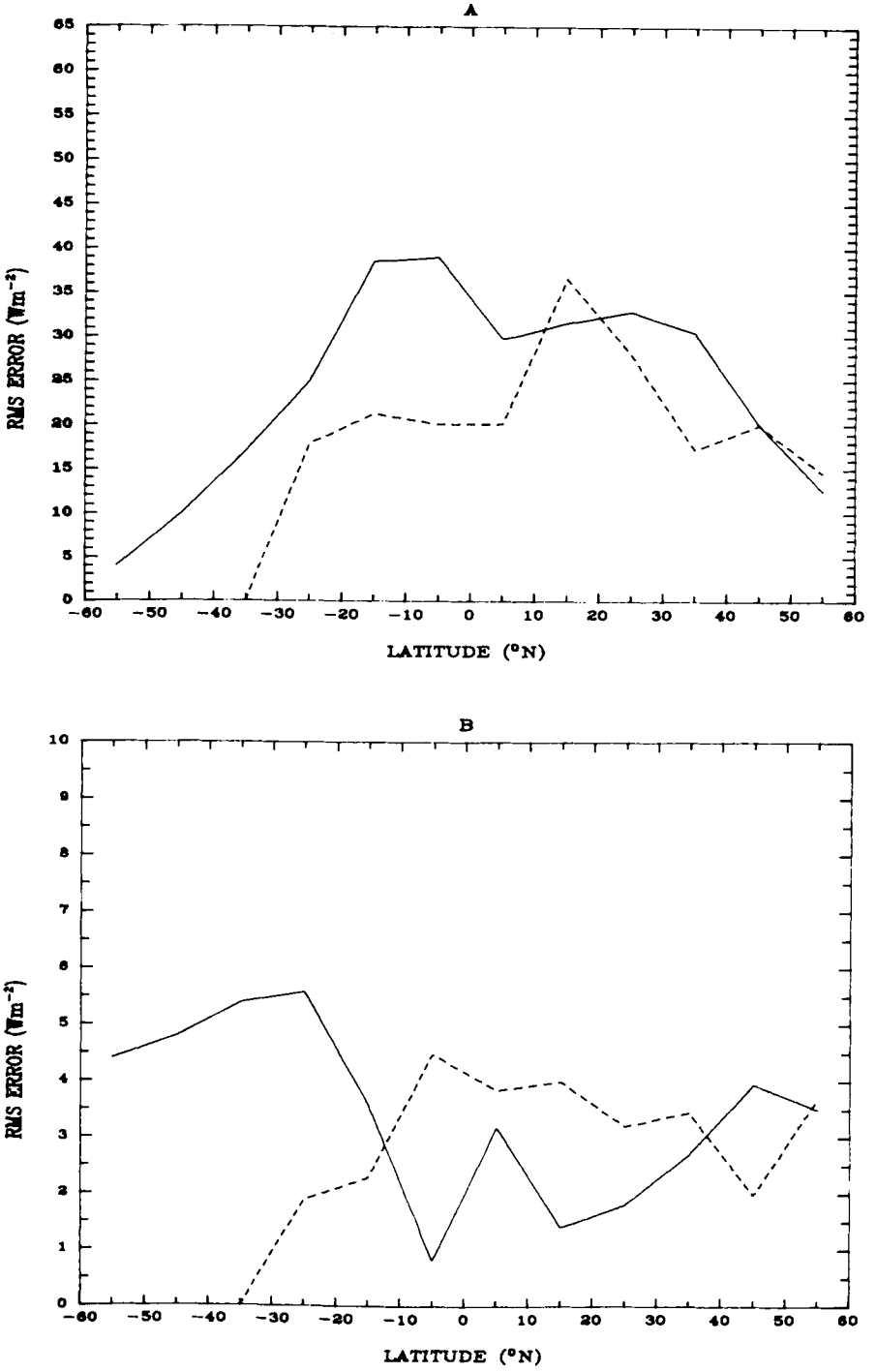

Fig. 2. Errors in radiation budget parameters due to sampling as a function of latitude. The results are produced for 5 degree square regions at 6-hourly sampling intervals. Solid line = over ocean, dashed line = over land. (a) Visible flux density, (b) Infrared flux density.

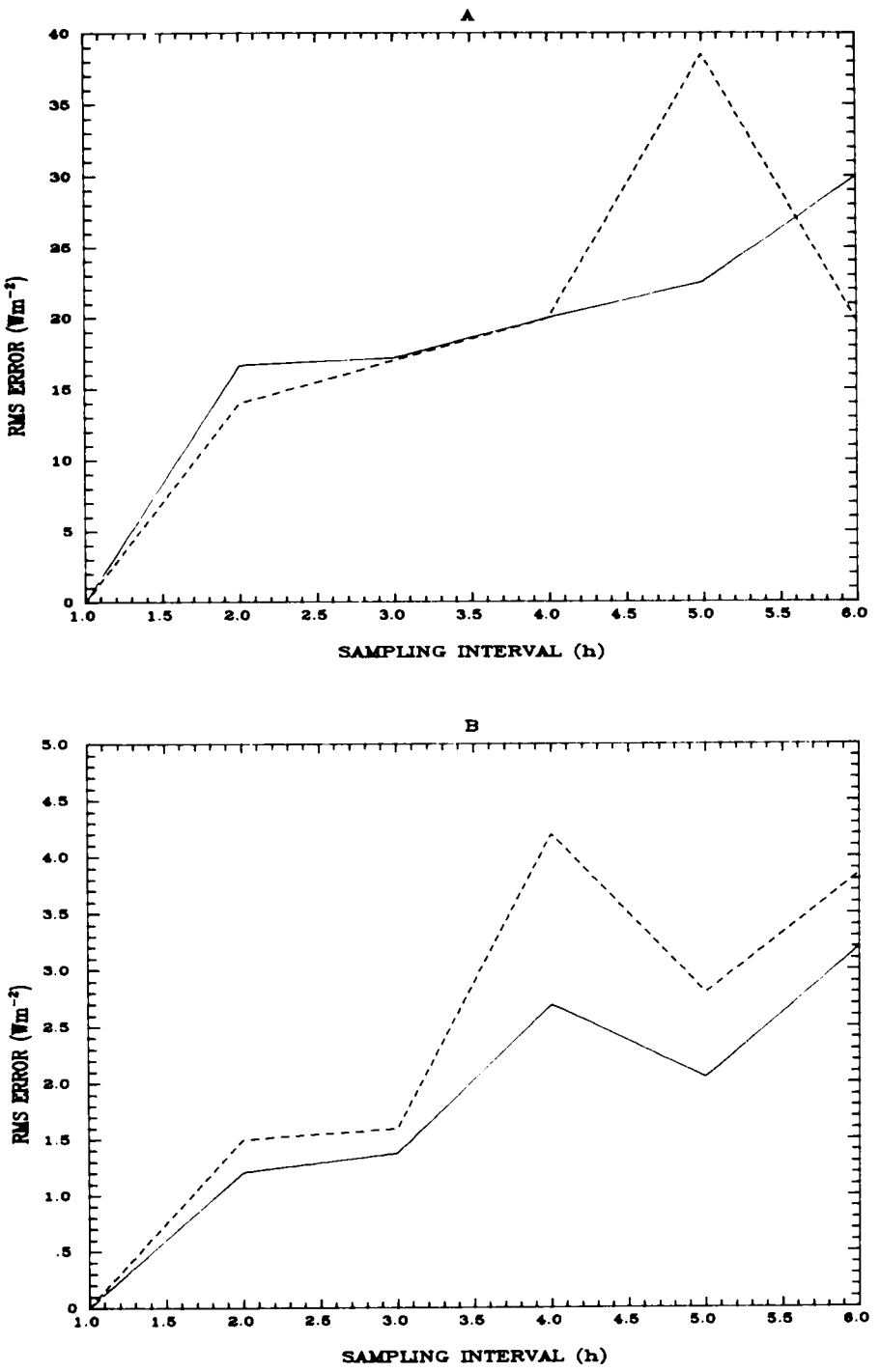

Fig. 3. Errors in radiation budget parameters due to changes in the sampling period for 5 degrees square areas at 5° N latitude. Solid line = over ocean, dashed line = over land. (a) Visible flux density, (b) Infrared flux density.

Table 1. *Variation of error for 6-hourly universal time sampling with time of first sample—for 5 × 5 degree areas for bin centred at 5° N*

Time	VIS (W m^{-2})	IR (W m^{-2})
0	30.0	2.9
1	48.9	2.8
2	49.2	2.4
3	53.9	3.1
4	60.7	3.9
5	68.9	5.0

square area in a latitude swath centred at 5°N. Since the errors will vary as $(n)^{-1/2}$, where n is the number of measurements, this variation would be expected to follow a quadratic curve. This is the general situation, with major deviations occurring only at higher sampling intervals, which are believed to be due to local time effects becoming apparent, as is shown in Table 1 where we have shown the variation of this error with the time of the first sample.

The jump in the values for the visible channel after the first measurement may be due to the reduction in the effective number of samples taken during the day. If the number of daylight hours is an integer multiple of 6, that is $6 \times n$, then starting at the first sample will give n measurements, whilst later starting times will only give $n - 1$ or less values. This effect is especially noticeable in the visible measurement, since the number of samples is lower than for the infrared, and the channel is strongly affected by the large diurnal variation of the available solar radiation.

Figs. 4a, b similarly show the decrease in error for the fluxes over different surfaces, in this case decreasing quadratically as the area increases. These figures show that a 5 × 5 degree square area is probably the largest area over which it is necessary to average radiation budget measurements to minimise the errors, owing to the rapid fall off in error at this scale. More interestingly, the nature of this variation suggests that advective processes are the dominant cause of error, as *in situ* processes will not show such a strong areal dependence (except in cases of organized convection, where the variation of error will decrease with area until the area is of the order of the mean area occupied by a convective cell).

4.2. *Local time sampling*

Figs. 5a, b show the effects of the different start times on making observations at fixed local time, for the visible and infrared 5 × 5 degree areas at 12-hourly intervals. The error in the infrared flux is again quite small, ranging from 4 to 7 W m^{-2}, with a minimum when sampling at 2 am and 2 pm. The errors in the visible flux are considerably larger, ranging from 36–140 W m^{-2}, and are in anti-phase to the infrared flux error, with a minimum when sampling at 9 am and 9 pm. This result indicates that the error is more directly related to the number of albedo measurements made, as around this period albedos are available for both measurement periods rather than just one, than to the proximity of the measurement to the maximum insolation.

The variation of error with spatial extent is similar to that demonstrated for universal time sampling, a 5 × 5 degree latitude/longitude area providing a maximum necessary area for averaging whilst maintaining spatial variability, although they are higher primarily due to the longer sampling interval. Fig. 6a, b show the latitudinal variation of error for 5 × 5 degree square areas with sampling at 9 am and 9 pm. These figures are again similar to their equivalents for universal time sampling over the ocean, with the exception that the ITCZ does not show up so significantly—probably because the sampling times are well away from the period of maximum convective activity. Over the land, this variation in the visible is superimposed on a general increase in error with latitude, reflecting higher variability over the northern hemisphere landmasses, due to the effects of fog at the surface and the complex weather patterns associated with depressions.

Fig. 7a, b show similar results with sampling at 6-hourly intervals, simulating a two satellite measurement system, as flown at present by NOAA. Sampling errors are much reduced, to less than 3 W m^{-2} for the infrared irradiance and 25 W m^{-2} for the visible. The time of the satellite overpass is less significant for a two satellite system, there being little difference between the errors at different sampling times. The similar magnitude of the universal and local time sampling errors for a 6 h interval confirms this result.

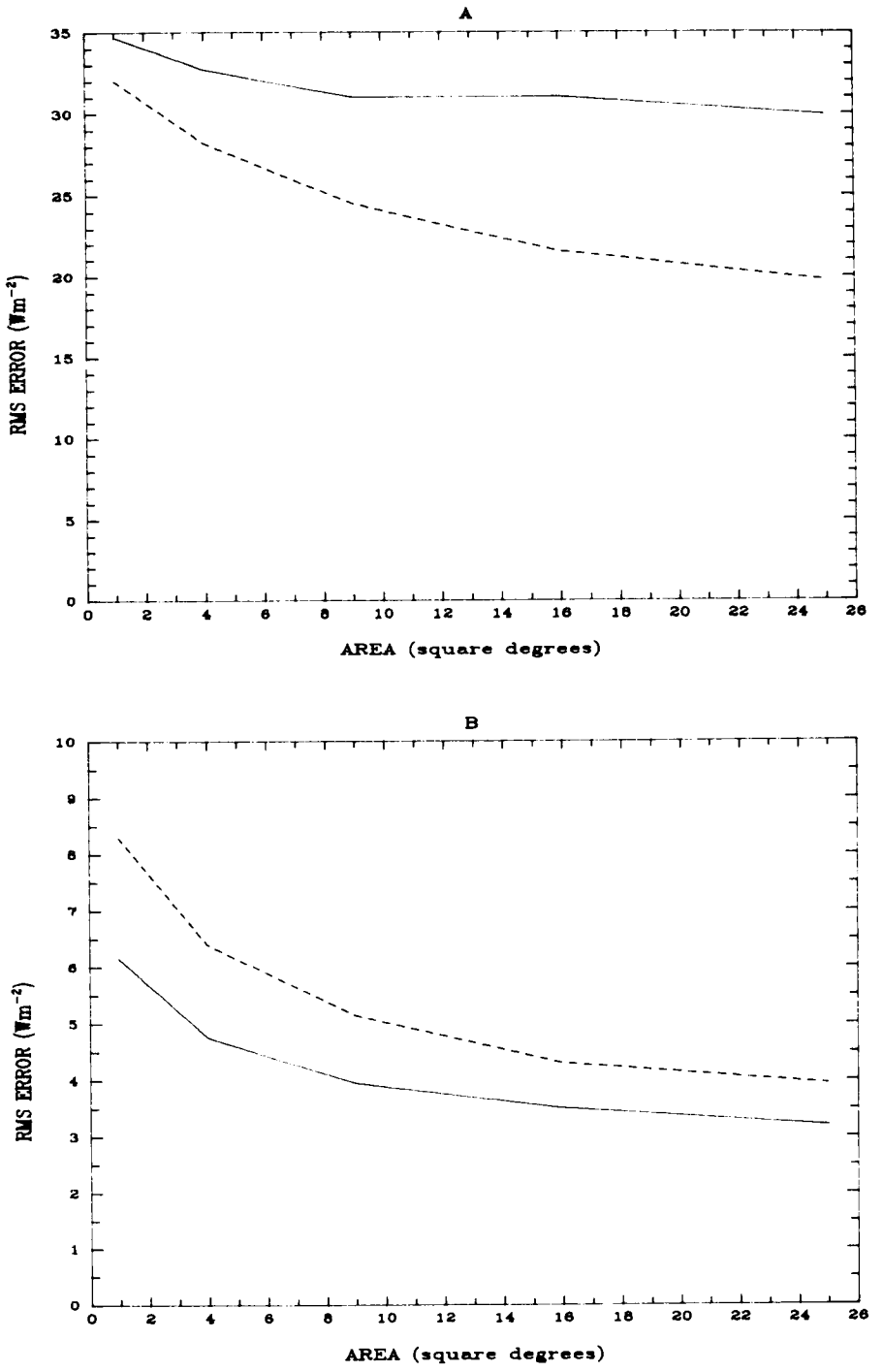

Fig. 4. Variation in the error in radiation budget parameters due to sampling as a function of spatial extent, at latitude 5° N. Solid line = over ocean, dashed line = over land. (a) Visible flux density, (b) Infrared flux density.

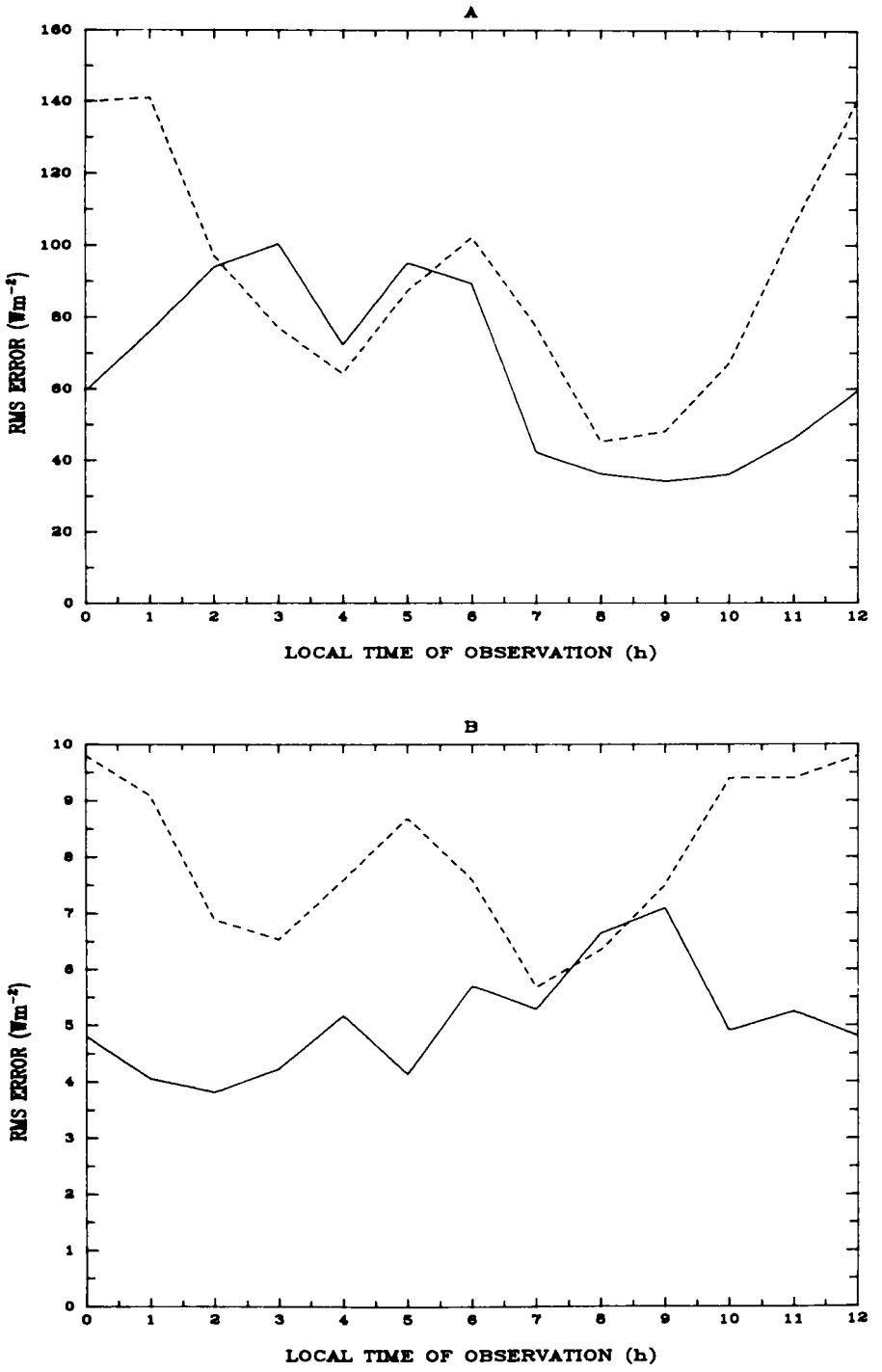

Fig. 5. Errors in radiation budget parameters due to sampling in local time as a function of sampling time for 12-hourly sampling. The results are for 5° N latitude. Solid line = over ocean, dashed line = over land.

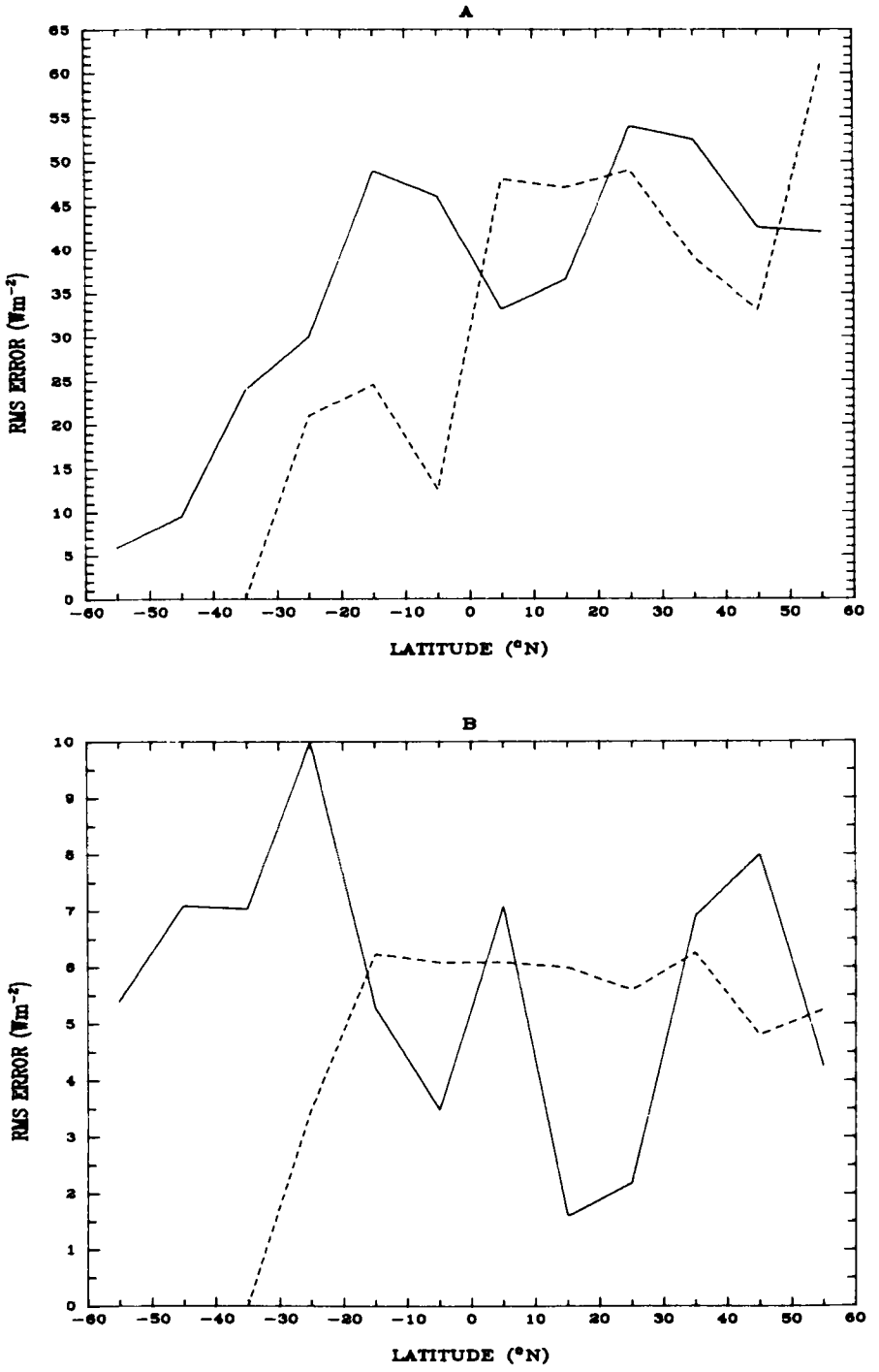

Fig. 6. Errors in radiation budget parameters due to sampling in local time as a function of latitude. The results are produced for 5 degree square regions at 12-hourly sampling intervals. Solid line = over ocean, dashed line = over land. (a) Visible flux density, (b) Infrared flux density.

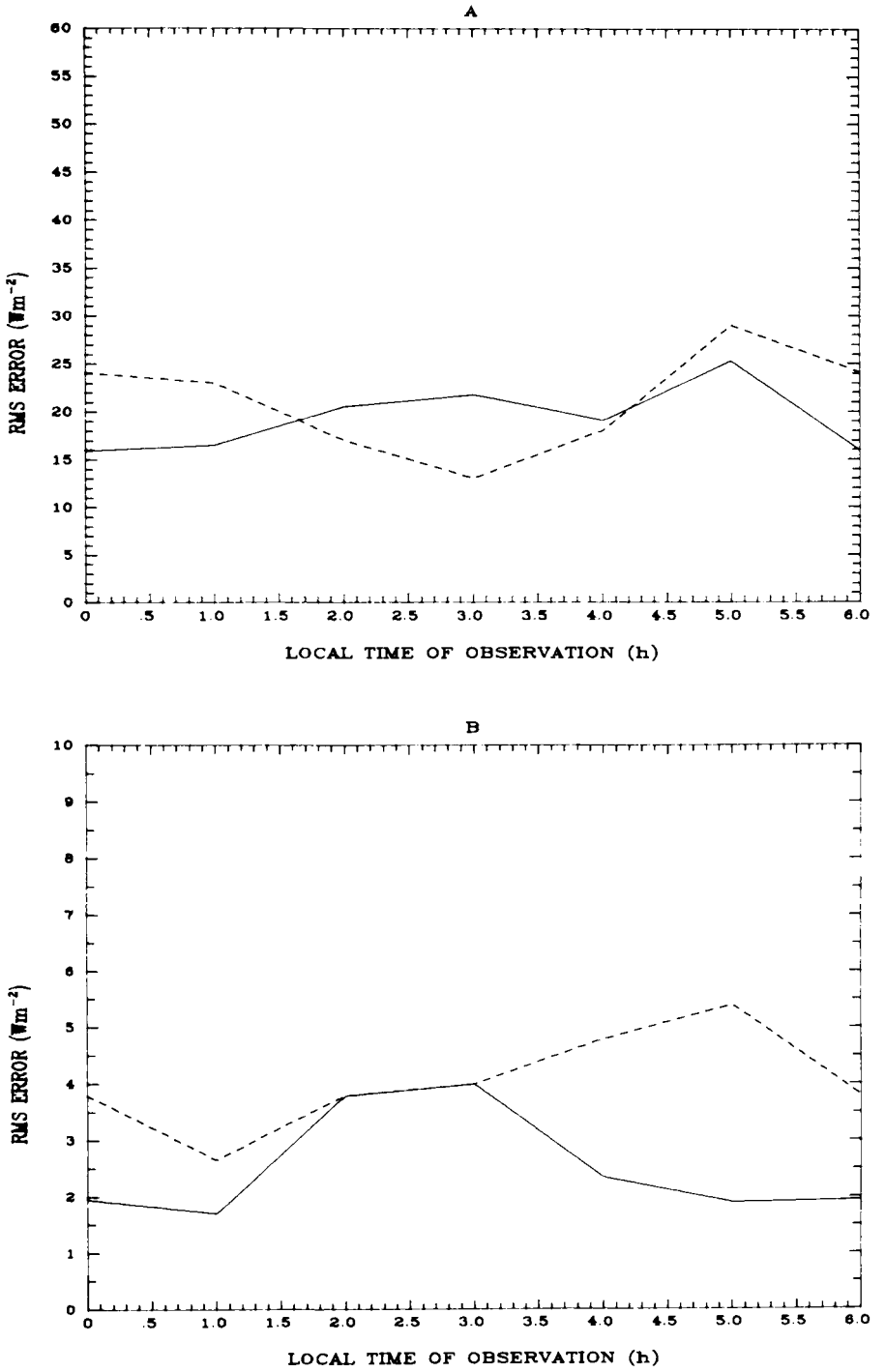

Fig. 7. Errors in radiation budget parameters due to sampling in local time as a function of sampling time for 6-hourly sampling. The results are for 5° N latitude. Solid line = over ocean, dashed line = over land.

5. Conclusion

This work has demonstrated that in order to minimise errors in estimations of the daily mean radiative fluxes on the Earth, data should, for the highest accuracy whilst retaining spatial information, be spatially averaged to areas of 5 × 5 degrees square, and shows the expected errors for reduced spatial areas. In addition, the errors due to sampling at different periods in universal time are presented, allowing the selection of a sampling interval to meet specific accuracy requirements when processing imagery derived from geostationary satellites. Furthermore, the errors inherent in polar orbiter sampling have been evaluated as a function of the local time of observation, and optimal sampling times discussed for both single and dual satellite observation systems. This work has also shown the importance of latitudinal effects on these errors, which may be directly related to the basic circulation regions (e.g. mid-latitude westerlies, ITCZ) and has produced representative values of this variation.

A significant factor which has emerged from this study is the dominating role of cloud variability in temporal sampling error. By direct comparison of measured cloud amounts to flux densities over small areas with differing cloud amounts we find that

$$\frac{d(\text{albedo})}{d(\text{cloud fraction})} = 0.2\text{–}0.4,$$

whilst

$$\frac{d(\text{IR})}{d(\text{cloud fraction})} = 20\text{–}50 \text{ W m}^{-2}.$$

Thus, if sampled at local noon, the difference in fluxes between a completely clear and a completely cloudy region would be

$$d_{\text{IR}} = 20\text{–}50 \text{ W m}^{-2},$$

$$d_{\text{VIS}} = 300\text{–}500 \text{ W m}^{-2}.$$

That is, an instantaneous visible change of 10–20 times that of the infrared, although the effect of this on a daily mean would be reduced by a factor of about 4, owing to the diurnal variation of the solar insolation.

A change from completely clear to completely cloudy is unlikely over the course of 6 h, for the sizes of area considered, although given the area covered by the samples it is bound to occur at some stage. However, smaller changes in cloudiness will produce similar relative changes. These values correspond very well with the relative magnitudes of error produced through temporal sampling.

These results indicate that the optimization of sampling periods and satellite overpass times for radiation budget estimates is primarily a matter of optimizing for the visible measurements, where the sampling error is typically more than 5 times that for the infrared observations. If a single polar orbiter radiometer system is used to derive these measurements, this visible error will be minimised if measurements are taken near 9 am and 9 pm, when two measurements of the albedo may be made, rather than the one available at other times.

6. Acknowledgement

This work is supported by the Natural Environment Research Council (UK).

REFERENCES

Gruber, A. and Winston, J. S. 1978. Earth-atmosphere radiative heating based on NOAA scanning radiometer measurements. *Bull. Amer. Meteorol. Soc. 59*, 1570–1573.

Minnis, P. and Harrison, E. F. 1984. Diurnal variability of regional cloud and surface radiative parameters derived from GOES data. Part III: November 1978. Radiation parameters. *J. Clim. Appl. Meteorol.*, in press.

Raschke, E. Vonder Haar, T. H., Bandeen, W. R. and Pasternak, M. 1973. The annual radiation budget of the earth–atmosphere system during 1969–70 from Nimbus 3 measurements. *J. Atmos. Sci. 30*, 341–364.

Saunders, R. W. and Hunt, G. E. 1983. Some radiation budget and cloud measurements derived from METEOSAT data. *Tellus 35B*, 177–188.

Saunders, R. W., Stowe, L. L., Hunt, G. E. and England, C. F. 1983. An intercomparison between radiation budget estimates from METEOSAT 1, Nimbus-7 and TIROS-N satellites. *J. Clim. Appl. Meteorol. 22*, 546–559.

Stephens, G. L., Campbell, G. G. and Vonder Haar, T. H. 1981. Earth radiation budget measurements from satellites and their interpretation for climate modelling and studies. *J. Geophys. Res. 86*, 9739–9760.

Taylor, V. R. and Stowe, L. L. 1984. Reflectance

characteristics of uniform earth and cloud surfaces derived from NIMBUS-7 ERB. *J. Geophys. Res. 89*, 4987–4996.

Vonder Haar, T. H. and Suomi, V. 1971. Measurements of the earth radiation budget from satellites during a five year period. Part I: Extended time and space means. *J. Atmos. Sci. 28*, 305–314.